The Astrophysical Journal Supplement Series, 173:392–403, 2007 December

ULTRAVIOLET THROUGH INFRARED SPECTRAL ENERGY DISTRIBUTIONS FROM 1000 SDSS GALAXIES: DUST ATTENUATION

Benjamin D. Johnson,[1] David Schiminovich,[1] Mark Seibert,[2] Marie Treyer,[3,4] D. Christopher Martin,[3] Tom A. Barlow,[3] Karl Forster,[3] Peter G. Friedman,[3] Patrick Morrissey,[3] Susan G. Neff,[5] Todd Small,[3] Ted K. Wyder,[3] Luciana Bianchi,[6] Jose Donas,[4] Timothy M. Heckman,[7] Young-Wook Lee,[8] Barry F. Madore,[2] Bruno Milliard,[4] R. Michael Rich,[9] Alex S. Szalay,[7] Barry Y. Welsh,[10] and Sukyoung K. Yi[8]
Received 2007 August 2; accepted 2007 September 3

ABSTRACT

The meaningful comparison of models of galaxy evolution to observations is critically dependent on the accurate treatment of dust attenuation. To investigate dust absorption and emission in galaxies we have assembled a sample of ∼1000 galaxies with UV through IR photometry from *GALEX*, SDSS, and *Spitzer*, and optical spectroscopy from SDSS. The ratio of IR to UV emission (IRX) is used to constrain the dust attenuation in galaxies. We use the 4000 Å break as a robust and useful, although coarse, indicator of star formation history (SFH). We examine the relationship between IRX and the UV spectral slope (a common attenuation indicator at high redshift) and find little dependence of the scatter on $D_n(4000)$. We construct average UV through far-IR spectral energy distributions (SEDs) for different ranges of IRX, $D_n(4000)$, and stellar mass (M_*) to show the variation of the entire SED with these parameters. When binned simultaneously by IRX, $D_n(4000)$, and M_* these SEDs allow us to determine a low-resolution average attenuation curve for different ranges of M_*. The attenuation curves thus derived are consistent with a $\lambda^{-0.7}$ attenuation law, and we find no significant variations with M_*. Finally, we show the relationship between IRX and the global stellar mass surface density and gas-phase metallicity. Among star-forming galaxies we find a strong correlation between IRX and stellar mass surface density, even at constant metallicity, a result that is closely linked to the well-known correlation between IRX and star formation rate.

Subject headings: dust, extinction — galaxies: evolution — galaxies: fundamental parameters — infrared: galaxies — ultraviolet: galaxies

1. INTRODUCTION

Measurement of the star formation history (SFH) of galaxies and the distribution thereof tests models of galaxy evolution. Such measurement requires the detailed treatment of dust attenuation, which poses one of the most severe obstacles to converting observed properties (e.g., broadband colors or line fluxes) into a SFH or star formation rate (SFR).

One of the primary tools for the measurement of dust attenuation, especially at high redshift, is the relation between the ratio of infrared flux to ultraviolet flux (IRX) and the ultraviolet spectral slope (β, where $f_\lambda \sim \lambda^\beta$). The former can be considered an approximate measure of the amount of dust attenuation, since the IR flux is produced by light absorbed at primarily UV wavelengths, while the UV flux measures the light transmitted at these wavelengths. The UV spectral slope measures the reddening (or color excess) of the UV spectrum due to selective absorption by dust—assuming that before attenuation the spectrum is nearly flat and relatively insensitive to the SFH. The utility of this relation lies in the relatively easy measurement of the rest-frame UV color for large samples of galaxies at $z > 1$, from which the attenuation can be inferred.

The calibration (and scatter) of this relation is of great interest for measurements of the SFR of galaxies at high redshift (especially those based on the rest-frame UV luminosity) and for the resulting estimates of the SFR density and its evolution (Madau et al. 1996; Schiminovich et al. 2005). This calibration is usually empirical, as is necessary at least in part because of the dependence of the reddening effect of the dust on the assumed properties of the dust (e.g., the extinction law and dust geometry). One must then assume that these dust properties do not evolve strongly with redshift, although calibrations based entirely on high-redshift galaxies may soon become available (Reddy et al. 2006).

Such empirical calibration, at any redshift, requires both rest-frame IR and UV observations galaxies. In the past such data have been available from *IRAS* and *IUE* for samples of nearby starbursting galaxies, where a strong correlation between IRX and β was found (Meurer et al. 1999). With the launch of *GALEX*, UV data has become available for a larger sample of more normal galaxies (Seibert et al. 2005; Buat et al. 2005), for which it appears that the relation between IRX and β is shifted to redder colors and has increased scatter. Similar results were obtained for a sample of individual OB associations by Bell (2002), who suggested that these effects were due to variations in the relative star-dust geometry (e.g., Witt & Gordon 2000). Kong et al. (2004) found a trend with the 4000 Å break (a coarse measure of the SFH) of the offset of starburst galaxies from the best-fit IRX-β

[1] Department of Astronomy, Columbia University, New York, NY 10027.
[2] Observatories of the Carnegie Institution of Washington, 813 Santa Barbara Street, Pasadena, CA 91101.
[3] California Institute of Technology, MC 405-47, 1200 East California Boulevard, Pasadena, CA 91125.
[4] Laboratoire d'Astrophysique de Marseille, BP 8, Traverse du Siphon, 13376 Marseille Cedex 12, France.
[5] Laboratory for Astronomy and Solar Physics, NASA Goddard Space Flight Center, Greenbelt, MD 20771.
[6] Center for Astrophysical Sciences, Johns Hopkins University, 3400 North Charles Street, Baltimore, MD 21218.
[7] Department of Physics and Astronomy, Johns Hopkins University, Homewood Campus, Baltimore, MD 21218.
[8] Center for Space Astrophysics, Yonsei University, Seoul 120-749, Korea.
[9] Department of Physics and Astronomy, UCLA, Los Angeles, CA 90095.
[10] Space Sciences Laboratory, 601 Campbell Hall, University of California, Berkeley, CA 94720.

relation. On the basis of spectral synthesis modeling, they thus ascribed the scatter and shifts toward redder colors in the IRX-β relation to the effect of SFH on β, in the sense that a large population of old stars will tend to produce a redder intrinsic, unattenuated UV color. The largest effects in the models were seen for significant old bursts superimposed on a smoother SFH. The spatial resolution of *GALEX*, combined with the spatial resolution of *Spitzer*, has allowed for the investigation of the IRX-β relation in detail in nearby, resolved galaxies (Boissier et al. 2004; Gil de Paz et al. 2006; Calzetti et al. 2005). One important outcome of this work is the suggestion that populations of different ages are obscured by differing amounts of dust (Calzetti et al. 2005), a result consistent with the findings of Charlot & Fall (2000) for global measures of attenuation. Such a scenario further complicates the interpretation of the IRX-β relation (Panuzzo et al. 2007). The combination of sensitive UV and IR observations of galaxies with *GALEX* and *Spitzer* has enabled the investigation of the IRX-β relation for large samples of galaxies (Buat et al. 2005; Cortese et al. 2006).

This paper is part of a series investigating the UV through IR properties of a large, well-defined sample of galaxies observed spectroscopically for SDSS and by *GALEX* and *Spitzer*. The additional diagnostics of stellar populations, SFR, and attenuation provided by the SDSS data make the sample presented here a unique and important test bed for the understanding of the IRX-β relation.

The large amount of homogenous ancillary information available from the SDSS observations, in addition to the UV and IR data, also allows us to investigate the effects of dust across the UV through near-IR spectrum. When such a wide range of wavelengths is considered, the effects of SFH on the spectrum become much more pronounced than they are for the UV spectrum alone (Johnson et al. 2007a). Indeed, optical colors are often used as a proxy for SFH (Bell et al. 2004; Faber et al. 2007), despite the potentially large additional contribution of attenuation to these colors. Here we present the global UV through IR spectral energy distributions (SEDs) of a large range of galaxy types. We show how these measured SEDs vary as a function of stellar mass, SFH, *and* attenuation. In particular, we use these SEDs to derive an "average" dust attenuation law and make a first attempt to determine the variation of this law (if any) with the stellar mass of the galaxy. These SEDs are complementary to the integrated UV through IR SEDs presented for the smaller samples of much more local, resolved galaxies presented by Gil de Paz et al. (2006) and Dale et al. (2005) and to the average UV through IR SEDs of higher redshift galaxies (Zheng et al. 2007).

Besides constraining the correction of derived physical values for dust attenuation, the relation of the dust attenuation to the SFH, SFR, and stellar mass may provide an additional constraint on models of galaxy evolution, as the attenuation should be proportional to the gas surface density $\Sigma_{\rm gas}$ and gas-phase metallicity Z (Wang & Heckman 1996; Bell 2003; Martin et al. 2007; Cortese et al. 2006). Models that self-consistently treat absorption and emission by dust are necessary and must be able to both predict the correct distribution of $\Sigma_{\rm gas}Z$ (as are given by the models of, e.g., Croton et al. 2006; De Lucia et al. 2006; Somerville et al. 2001) *and* convert this quantity into a dust attenuation curve to accurately predict the UV through IR properties of galaxies. We investigate the relation between $\Sigma_{\rm gas}Z$ and attenuation for the galaxies in our sample that have metallicity measurements.

2. DATA

In this study we use optical spectroscopic and photometric observations of galaxies from SDSS, UV observations of these galaxies from *GALEX*, and IR observations of these galaxies from *Spitzer*. Readers are referred to Johnson et al. (2007a) for details of the data reduction and sample definition. Here we provide a summary of the sample properties and briefly describe several parameters derived from the data that are used throughout this analysis.

TABLE 1
Observations

Field Name	Size (deg^2)	$N_{\rm obs}$	$N_{\rm det}$ f, $n < 25$	$N_{\rm det}$ $m_{24} < 19.5$	$N_{\rm smpl}$
Lockman Hole	~9	872	792	819	721
FLS..........................	~3	186	147	158	118

The sample consists of galaxies targeted spectroscopically by SDSS (thus having a magnitude $r < 17.7$), for which a stellar mass has been determined by Kauffmann et al. (2003a) and which have been observed by both *GALEX* and *Spitzer*. This sample is located in two regions of the sky, the Lockman Hole (observed by *Spitzer* as part of the SWIRE survey) and the *Spitzer* Extragalactic First Look Survey (FLS). Table 1 gives the number of galaxies observed in each field and the detection rates. The sample properties (redshift, stellar mass, and morphological distribution, etc.) are very similar to the sample of Kauffmann et al. (2003a), although the redshift distribution is less smooth due to the presence of groups, filaments, and sheets in the spatial distribution of galaxies in these fields. The median redshift of the sample is $z = 0.11$, with a maximum of $z < 0.305$. The median stellar mass (see below) is $\log M_* = 10.7\ M_\odot$ with a range of $8.45 < \log M_* < 11.91$. The SFR range is $\sim$0.01–60 $M_\odot$ yr^{-1} (Johnson et al. 2007b; Brinchmann et al. 2004). A detailed investigation of the morphological properties of the sample is beyond the scope of this work, but we note that irregular, elliptical, and spiral galaxies of various inclinations (face-on through edge-on) are included (see Johnson et al. 2007a, Fig. 4). The SDSS spectroscopic galaxies with stellar masses from Kauffmann et al. (2003a) that are *not* detected in the UV or IR are $\sim$30% of galaxies on the red sequence and a few blue, low stellar mass dwarf galaxies that are missed primarily because we require objects to have Petrosian radii in the r band of less than 11″ and redshift $z > 0.02$, ensuring accurate photometry. Photometry is from the modified SExtractor output for the *GALEX* far-UV (f, $\lambda \sim 1528$ Å) and near-UV (n, $\lambda \sim 2271$ Å) data, SDSS Petrosian magnitudes (*ugriz*) for the optical data, and large aperture photometry for the *Spitzer* data (with a 7″ radius in the IRAC 3.6 through 7.8 μm bands, a 12″ radius at 24 μm, and a 16″ radius at 70 μm where the sources are largely unresolved). The f through 3.6 μm magnitudes are K-corrected to $z = 0.1$ (the median redshift of the sample) via the method of Blanton & Roweis (2006), with the result denoted with a superscripted 0.1, e.g., $^{0.1}u$. We also determine K-corrections of the f and n magnitudes to $z = 0.0$ ($^{0.0}f$, $^{0.0}n$) for comparison to more local galaxies (§ 3.2).

In this work we are interested in the stellar masses derived by Kauffmann et al. (2003a) and the metallicities derived by Tremonti et al. (2004). These properties have been made available as catalogs by these authors.[11] The stellar masses are derived from the z-band SDSS photometry. The mass-to-light ratio in that band is obtained for each galaxy from fits of stellar population synthesis models to the optical spectrum, in particular the 4000 Å break strength and the Hδ absorption strength, $H\delta_A$. The gas-phase metallicities are derived from the SDSS measured emission lines

[11] http://www.mpa-garching.mpg.de/SDSS.

for galaxies with strong emission lines that do not show evidence of AGN activity in the optical (see Tremonti et al. 2004 for details). We also consider in § 6 the SFR derived by Brinchmann et al. (2004) from a comparison of measured optical emission lines to a large suite of models of galaxy spectra.

2.1. $D_n(4000)$

The 4000 Å break strength, here defined as in Balogh et al. (1999) $D_n(4000)$, is a useful indicator of the mass-to-light ratio, since it is sensitive to the SFH. Larger $D_n(4000)$ signifies, approximately, a larger ratio of old stars to young stars. This break is measured at high signal-to-noise ratio (S/N) for all of the galaxies in the sample and is not very sensitive to the presence of dust attenuation (but see MacArthur 2005). $D_n(4000)$ is only measured within the 3″ radius spectroscopic aperture of the SDSS and can therefore be overestimated for galaxies with moderate bulge/disk ratios (Kauffmann et al. 2006). $D_n(4000)$ serves as our primary measure of SFH.

2.2. *IRX*

The combination of UV and IR data allows us to construct a robust measure of attenuation: the so-called infrared excess, IRX $= \log(L_{\rm dust}/L_{\rm uv})$. We define $L_{\rm uv} = \nu L_\nu$, where $\nu = c/1390$ Å ($\lambda = 1390$ Å is the effective wavelength of the $^{0.1}f$ band) and calculate L_ν from the K-corrected absolute magnitude, assuming the redshift-distance relation given by a concordance cosmology with $\Omega_m = 0.3$, $\Omega_\Lambda = 0.7$, $H_0 = 70$ km s^{-1} Mpc^{-1}. $L_{\rm dust}$, the 8–1000 μm luminosity, is estimated from the 24 μm luminosity as in Johnson et al. (2007a), with a bolometric correction that depends on the ratio of 8 to 24 μm fluxes. These bolometric corrections are derived from the models of Dale et al. (2001).

If the IR emission traces the (predominantly blue) light from (predominantly) young stars that is absorbed by dust and reradiated, and the UV emission traces the light from young blue stars that is transmitted, then their ratio is a measure of the optical depth. The UV attenuation in magnitudes can be written in terms of IRX, including a parameter η to account for light absorbed by dust at wavelengths other than the UV, as

$$\hat{A}_{\rm IRX} = 2.5 \log\left(\eta 10^{\rm IRX} + 1\right), \qquad (1)$$

with $\eta = 1/1.68$ (Meurer et al. 1999; Johnson et al. 2007b). Other conversions between IRX and attenuation are available (e.g., Bell 2002; Buat et al. 2005), but they are consistent with this formulation, which is physically motivated and simply understood. However, this formulation relies on a number of simplifying assumptions. First, the fraction of light absorbed by dust at wavelengths other than $\lambda \sim 1390$ Å may depart from the canonical value of 1–1/1.68, depending especially on the SFH of the galaxy (see, e.g., Johnson et al. 2007b)—this will change the relation between $\hat{A}_{\rm IRX}$ and the true attenuation at 1390 Å, A_{1390}. Related to this, different stellar populations *within* a galaxy may be attenuated by different amounts of dust (Charlot & Fall 2000; Calzetti et al. 2005). Second, the relative geometry of the stars and dust can lead to the misestimation of A_{1390} by $\hat{A}_{\rm IRX}$, with an extreme example given by a group of stars surrounded by a ring of dust normal to the line of sight (Bell et al. 2002). This effect has been examined in detail by Witt & Gordon (2000), Buat & Xu (1996), Gordon et al. (2000), and Pierini et al. (2004). Nevertheless, IRX is a qualitatively different measure of attenuation from ones that rely on a color excess (e.g., the Balmer decrement; Kennicutt 1998a and references therein).

3. ATTENUATION FROM THE IRX-β RELATION

The relation between dust attenuation and UV color, the IRX-β relation (where β gives the power-law exponent of the UV spectrum, $f_\lambda \sim \lambda^\beta$) is a common tool for the analysis of the attenuation in galaxies at high redshift (and low). The rest-frame UV color is more easily measured at high redshift, where it is redshifted into the optical, than many other diagnostics (e.g., the Balmer decrement). However, at low redshift the calibration has been restricted until recently to galaxies with very high SFR (Meurer et al. 1999). A number of more recent studies have suggested that the relation becomes significantly scattered when extended to less rapidly star forming galaxies, or even to individual OB associations, and is shifted to redder UV color (Bell et al. 2002; Seibert et al. 2005; Cortese et al. 2006; Gil de Paz et al. 2006; Boissier et al. 2006; Dale et al. 2005). Kong et al. (2004) suggest, on the basis of stellar population synthesis modeling, that the increased scatter and the shift to redder UV color may be due to the effect of SFH on β. Bell (2002) argue that these effects are due to radiative transfer through nontrivial dust geometries. Panuzzo et al. (2007) find that differing attenuation of stellar populations with different ages can lead to significant changes in the location of galaxies in the IRX-β plane.

3.1. *IRX-β a Function of $D_n(4000)$*

We construct an analog of the IRX-β relation for our sample galaxies. We use $^{0.1}(f - n)$ color as a proxy for β, since we lack UV spectra–see Kong et al. (2004) for a comparison of β derived from *GALEX* colors and from spectra. In the left panel of Figure 1 we show the relation between IRX and $^{0.1}(f - n)$ color for different ranges of $D_n(4000)$. We find that the overall scatter in the IRX-β relation is much reduced compared to Johnson et al. (2006). This is due to the much smaller errors in UV color with the >10 times deeper UV data presented here. However, there is still no clear trend of the scatter in the IRX-β relation with $D_n(4000)$ (our chosen SFH indicator) for $D_n(4000) < 1.7$. Such an effect is constrained by these data to be quite small for low $D_n(4000)$, although it may also be masked by a strong dependence of the conversion between IRX and the true attenuation on $D_n(4000)$ (Johnson et al. 2007b).

As seen in Johnson et al. (2006), for $D_n(4000) > 1.7$ the scatter in the relation is greatly increased and the galaxies have in general much redder UV color than they do for $D_n(4000) < 1.7$. Gil de Paz et al. (2006) see a similar scatter in very UV red galaxies. There is no strong dependence of the behavior at $D_n(4000) > 1.7$ or $D_n(4000) < 1.7$ on the SFH indicator being used (e.g., the Hα equivalent width; see Johnson et al. (2007b) for examples of additional SFH indicators available for this sample).

We also show in Figure 1 the expectation for the relation between $\hat{A}_{\rm IRX}$ and $^{0.1}(f - n)$ color for a variety of dust models drawn from Witt & Gordon (2000). See Johnson et al. (2007a) for a detailed description of these models and their implementation in these color-color diagrams. Note that no single model matches the data clearly—in particular, models including a Milky Way–like extinction curve are strongly disfavored. The 2175 Å bump in such extinction laws, thought to be due to absorption by polycyclic aromatic hydrocarbon (PAH) molecules (Draine & Li 2006), leads to very little reddening of the UV color with IRX and perhaps even *bluer* colors with increasing attenuation. Note that small variations between galaxies of the particular star/dust geometry, as well as the dust *extinction* law, can easily lead to significant scatter in the IRX-β diagram. One must also consider here the possible effects of a dust attenuation optical depth that varies within the galaxy as a function of the stellar population (Charlot

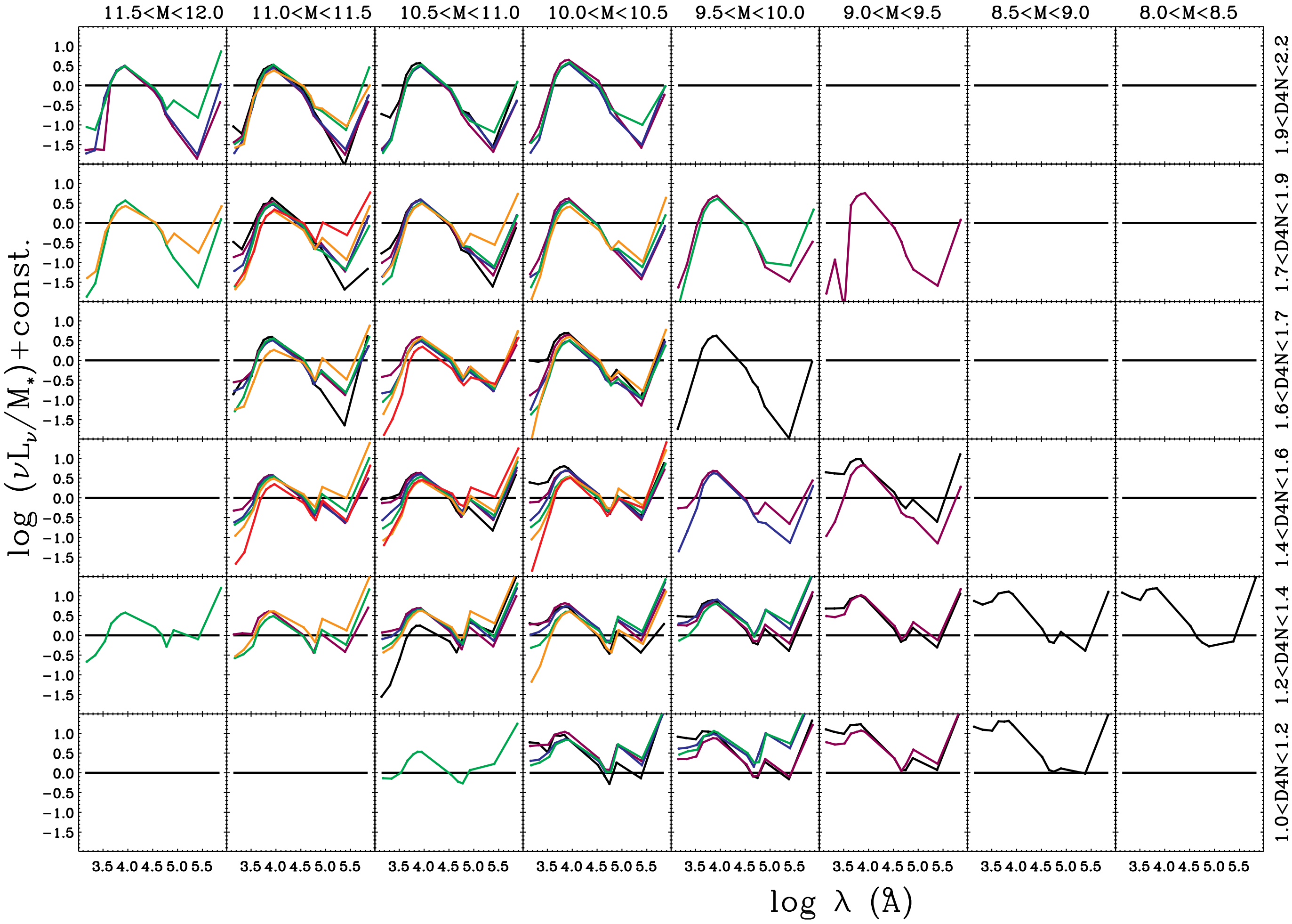

FIG. 5.—SEDs for different bins of stellar mass [given as $\log(M_*/M_\odot)$] and $D_n(4000)$, analogous to a color magnitude diagram. Within each of these stellar mass and $D_n(4000)$ bins the SEDs are normalized by stellar mass and further binned by $\hat{A}_{\rm IRX}$. See text for details and the definition of the parameter bins. The value of $\log(M_*/M_\odot)$ increases from left to right, while $D_n(4000)$ increases from bottom to top. The color of each average SED encodes the $\hat{A}_{\rm IRX}$ bin (*black*, *purple*, *blue*, *green*, *orange*, and *red*, respectively) for the six bins defined by $\hat{A}_{\rm IRX}$ = [0.0, 1, 2.0, 2.5, 3.5, 4.5, and 5.5].

and the attenuation at a given wavelength may then be written in terms of the attenuation at another wavelength as $A_{\lambda_2} = A_{\lambda_1}[G(\lambda_2)/G(\lambda_1)]$.

The color of a galaxy, $c_{\lambda_1,\lambda_2} = m_{\lambda_1} - m_{\lambda_2}$, where m_λ is the magnitude at wavelength λ, is given by the intrinsic color c_o plus the difference in the effective attenuation at each wavelength:

$$c_{\lambda_1,\lambda_2} = c_o + (A_{\lambda_1} - A_{\lambda_2}),$$
$$= c_o + A_{\lambda_1}[1 - G(\lambda_2)/G(\lambda_1)].$$

We make the (large) assumption that $\hat{A}_{\rm IRX} = A_{\lambda_1} = A_{1390\,\text{Å}}$. Assuming that c_o is relatively constant between galaxies for narrow ranges of $D_n(4000)$, the slope of the relation between the $^{0.1}(f - m_{\lambda_2})$ color and $\hat{A}_{\rm IRX}$, for a narrow range of $D_n(4000)$, then gives $1 - G(\lambda_2)/G(1390\ \text{Å})$. This relation is effectively shown in Johnson et al. (2007a) for several different colors and ranges of $D_n(4000)$, although IRX was used instead of $\hat{A}_{\rm IRX}$ and many of the colors used $^{0.1}n$ instead of $^{0.1}f$. We split the sample into bins of $D_n(4000)$ (=[1.0, 1.2, 1.3, 1.4, 1.5]) and determine the slopes for each color using the ordinary least-squares bisector (Isobe et al. 1990). In Figure 6 we show the resulting derived $G(\lambda_2)/G(1390\ \text{Å})$ for the different ranges of $D_n(4000)$. Errors are determined from the range in the slopes derived by fitting $\hat{A}_{\rm IRX}$

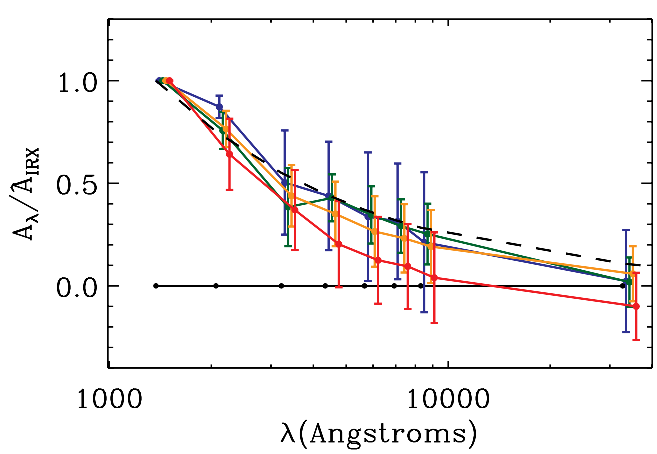

FIG. 6.—Derived $A_\lambda/\hat{A}_{\rm IRX}$ (i.e., the dust attenuation law; § 5) for different ranges of $D_n(4000)$ ($D_n(4000)$ = [1.1, 1.2, 1.3, 1.4, 1.5]; *blue to red*). The dashed line shows a $\lambda^{-0.7}$ attenuation curve. Galaxies are restricted to $9.5 < \log(M_*/M_\odot) < 11.5$. The curves are shifted slightly in wavelength for clarity.

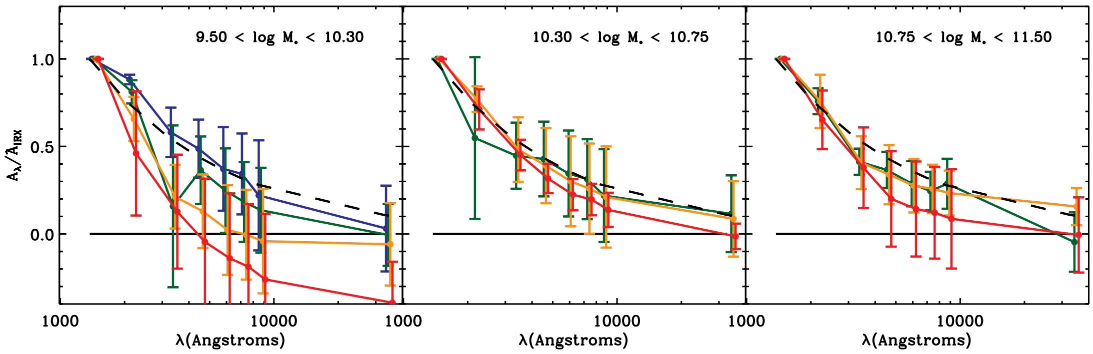

FIG. 7.—Same as Fig. 6, but showing the derived $A_\lambda/\hat{A}_{\rm IRX}$ (§ 5) for different ranges of $D_n(4000)$ ($D_n(4000) = [1.1, 1.2, 1.3, 1.4, 1.5]$; *blue to red*) and stellar mass. Each panel shows a different stellar mass range. We only show those mass and $D_n(4000)$ ranges for which there are >10 galaxies. The dashed line shows a $\lambda^{-0.7}$ attenuation curve. The curves are shifted slightly in wavelength for clarity.

given ${}^{0.1}(f - m_{\lambda_2})$ and vice versa. The resulting attenuation curves are consistent with a $\lambda^{-0.7}$ attenuation law.

There are a number of caveats to this method for the determination of the dust attenuation law. Primarily, $\hat{A}_{\rm IRX}$ is not the true $A_{1390\,\text{Å}}$, especially for galaxies with redder intrinsic spectra. This is likely the reason for the differing shapes of the attenuation curves for different ranges of $D_n(4000)$. This analysis does not exploit the unique advantage of IRX as a dust indicator, i.e., that the IR emission constrains the total absorbed flux. Indeed, the assumption that $\hat{A}_{\rm IRX} = A_{1390\,\text{Å}}$ is inconsistent with the fact that the derived attenuation laws are nonzero at longer wavelengths, which means that galaxies with different $D_n(4000)$ are likely to have different η (eq. [1] and Johnson et al. 2007b). Second, $G(\lambda)$ may not be separable from C (i.e., the shape of the attenuation curve may be dependent on the total amount of attenuation; this can happen due to geometric effects as shown by Witt & Gordon 2000). Another possible systematic error is that the unreddeded spectra may be determined by more than just $D_n(4000)$ (e.g., metallicity, contamination due to aperture effects)—c_o may not be constant even in small ranges of $D_n(4000)$, especially for colors based on the flux far from the 4000 Å break.

Another caveat to the method described above is that $G(\lambda)$ may not be universal, for example, because of a variation in the extinction law between galaxies. Such a variation might be expected if the composition of the dust causing the attenuation varies between galaxies. Dust composition may vary with metallicity, which is correlated with stellar mass. In particular, the 2175 Å bump in the Milky Way extinction curve, which is not seen in the LMC and SMC extinction curves, is thought to be due to PAH molecules (Draine & Li 2006)—these molecules have been shown to be underabundant in low-metallicity dwarf galaxies, although the reason for this is still unclear. A variation in the attenuation law with mass would be of special importance for interpreting the location of galaxies in the specific SFR–stellar mass plane in terms of SFHs (Labbe et al. 2007; Noeske et al. 2007) and for comparison of UV-derived SFRs to Hα-derived SFRs (e.g., Salim et al. 2007). For these reasons we consider the attenuation laws derived as above but for bins of $D_n(4000)$ *and stellar mass* (i.e., cells in Fig. 5). These are shown in Figure 7. The smaller number of galaxies in each bin results in a weaker constraint on $G(\lambda_2)/G(1390\text{Å})$ than in Figure 6. No significant trends with stellar mass are seen, although the uncertainties are large. A larger sample of galaxies is required to accurately test this hypothesis and, in addition, split the sample into, e.g., bins of $\hat{A}_{\rm IRX}$ to explore the coupling of attenuation law shape to the amount of attenuation in galaxies.

6. ATTENUATION AS A FUNCTION OF METALLICITY AND SURFACE BRIGHTNESS

At the local level the amount of dust attenuation is due to the column density of dust, $\tau = \int \sigma_{\rm dust} n_{\rm dust} \ell$, where $\sigma_{\rm dust}$ is the absorption cross section, $n_{\rm dust}$ is the dust volume density, and ℓ is the unit path length along the line of sight (e.g., Wang & Heckman 1996). Simplistically, one might write $n_{\rm dust}\ell = \Sigma_{\rm gas} f_{\rm dust}$, where $f_{\rm dust}$ is the global dust-to-gas ratio and $\Sigma_{\rm gas}$ is the column density of gas along the line of sight to the star or cluster of stars. We assume that $f_{\rm dust} \propto Z$, where Z is the gas-phase metallicity. We obtain Z from the log O/H values of Tremonti et al. (2004) via the solar values $(\log {\rm O/H})_\odot = 8.69$ and $Z_\odot = 0.02$, assuming that the oxygen abundance is a tracer of the total metal abundance within a factor of 2 or 3. In semianalytic modeling it is typical to make the assumption $f_{\rm dust} \propto Z$ and, furthermore, to use the global values of gas density and metallicity (Somerville et al. 2001; Martin et al. 2007). This approach involves several other assumptions: that the effect of stars being embedded *within* the gas can be neglected, that spatial variations in both gas surface density and metallicity are such that their product averages to the global value, and that all stars (of all ages) are affected equally. Such a relation between surface density, metallicity, and attenuation has been investigated empirically, using global quantities of resolved galaxies, by Boissier et al. (2006) and Cortese et al. (2006).

We consider here the relation of the globally measured attenuation to the global metallicity and surface density for the sample galaxies. We do not have measurements of the gas surface density and use instead the stellar mass surface density. Following Kauffmann et al. (2003b) this is calculated as $\Sigma_{*,z} = 0.5 M_*/(\pi R_{50}^2)$, where M_* is given by Kauffmann et al. (2003a) and R_{50} is the radius (in kpc) enclosing 50% of the Petrosian light in the z band. Bell (2003, Appendix B; see also Calzetti et al. 2007, Appendix A.1) makes a quantitative estimate of the relation in this case, obtaining

$$\tau_{\rm fuv,1550} = 1.7\eta Z f_g/(1 - f_g)\Sigma_*, \qquad (11)$$

where $\tau_{\rm fuv,1550}$ is the optical depth at 1550 Å, Z is the metallicity, f_g is the gas fraction, Σ_* is the stellar mass surface density, and η is a factor of order unity (Bell 2003; determine $\eta = 0.7$ to fit the attenuation-luminosity correlation) to account for, e.g., relative star dust geometry. Using the approximation $\tau_{\rm fuv} = \tau_{\rm fuv,1550}(1390/1550)^{-0.7}$ and equation (1), $\tau_{\rm fuv,1550}$ can be related to IRX.

In Figure 8 we show three projections of the relation between IRX, gas-phase metallicity, and $\Sigma_{*,z}$. The number of galaxies for which this is possible is small (219), due to the lack of metallicity

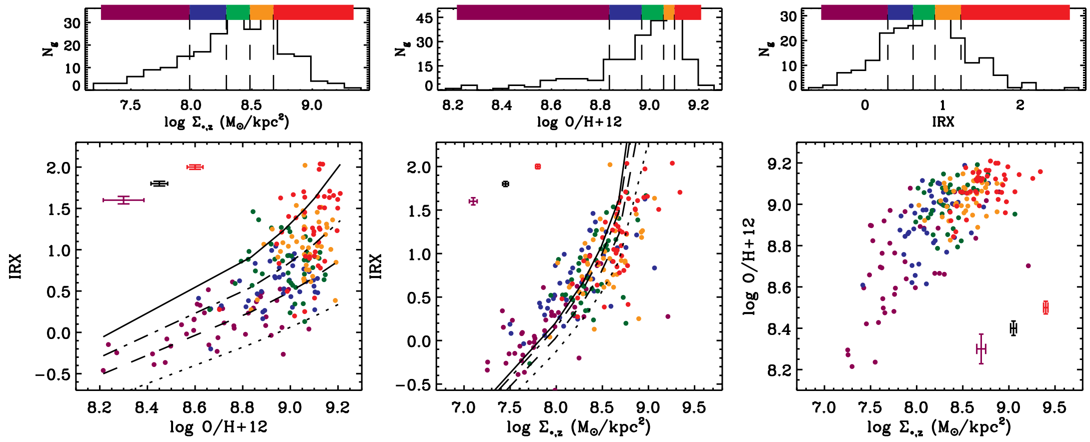

Fig. 8.—Three projections of the relation between IRX, gas-phase metallicity, and surface mass density for the 219 galaxies of the sample for which metallicity measurements are available from Tremonti et al. (2004). In each large panel the color coding is given by the quintiles of the distribution shown above that panel. In the left panel the black lines show (*bottom to top*) the relation of IRX to metallicity expected from eq. (11) for the values of $\Sigma_{*,r}$ that define, in increasing order, the limits of the bins used for the color coding. In the middle panel the lines are similar but here the metallicity is fixed at the limits of the bins used for the color coding.

measurements—these galaxies have strong emission lines and typically have large ratios of recent to past star formation. Note also that AGN identified in the optical spectra on the basis of emission-line ratios are excluded from this sample with metallicity measurements (Tremonti et al. 2004). The left and center panels show that there is a strong correlation between IRX and $\Sigma_{*,z}$, even when the metallicity is held nearly constant; metallicity and surface mass density are also correlated with each other, as shown in the right panel. Cortese et al. (2006) found a similar trend of IRX with *H*-band surface brightness (a close proxy for stellar mass surface density), although they did not simultaneously control for metallicity. The correlation of IRX with metallicity is very weak for constant surface mass density. However, there is an overall correlation of IRX with metallicity induced primarily by the correlation of metallicity with surface mass density. The lines in Figure 8 show those expected from equation (11), for the quintiles of the parameter used for the color coding (i.e., points of a certain color should fall between two adjacent lines). We have assumed $f_g = 0.1$ and require $\eta = 0.7$ to fit the data reasonably—this relation is very sensitive to the choice of η. The lines in the middle panel, for different quintiles of the metallicity distribution, show that the effect of the metallicity variations is *expected* to be weaker than the surface mass density variations, since the range of metallicity is only 1 order of magnitude, while the range in surface mass density is 2 orders of magnitude. Note that the shallower-than-expected slope of the data in this panel may well be due to the anticorrelation of f_g, which we have assumed to be constant, with surface density.

Indeed, it is possible to estimate Σ_g from the SFR density, assuming that the relation of Kennicutt (1998b) holds globally for these galaxies. Gas densities are calculated via

$$\Sigma_{g,k} = 10^6\left[\left(10^4/5\right)\mathrm{SFR}_e/\left(\pi R_{50}^2\right)\right]^{-1.4} M_\odot\ \mathrm{kpc}^{-2}, \quad (12)$$

using the median SFR derived by Brinchmann et al. (2004) and R_{50} as above (the conclusions are unchanged if we instead use the *u*-band half-light radius as an estimate of the extent of star formation). The mean of the ratio $\Sigma_{g,k}/\Sigma_{*,z}$ is approximately 0.16 (hence the assumption $f_g = 0.1$ made above). There is a significant trend of this ratio with surface mass density $\Sigma_{*,z}$, such that galaxies with larger $\Sigma_{*,z}$ have lower $\Sigma_{g,k}/\Sigma_{*,z}$; $\Sigma_{g,k}$ spans a much smaller range than $\Sigma_{*,z}$. This explains the steeper slope predicted by equation (11).

These results may be compared to those of Boissier et al. (2006), who found a correlation of IRX with metallicity (see also Boissier et al. 2004; Heckman et al. 1998). These studies did not consider the simultaneous effect of the surface density–metallicity correlation, and a trend with metallicity may thus be due to this additional component of the optical depth. What is perhaps more puzzling is that Boissier et al. (2006) did not find a good correlation between the local IRX and the local H I(+H_2) surface density (but see Buat & Xu 1996 and Xu et al. 1997). The relation between gas surface density and stellar surface density is highly scattered and poorly constrained, although we have assumed that the global values are simply related by f_g. If the stellar surface mass density is better correlated with IRX than the gas surface density, we must ask why. Is the stellar mass density tracing the *history* of metal and dust production, such that higher densities naturally lead to higher attenuations? This would seem to be accounted for by considering narrow ranges of metallicity. One component of the analysis that we have treated only superficially is that stars are necessary to measure IRX, and hence the attenuation—a region of large gas and dust column will not contribute to the measured attenuation if there are few stars; and, conversely, a large number of stars in a low dust column region will cause a low measured IRX, even if the global gas and dust surface density is large. IRX in fact measures the sum of the local $\Sigma_{\mathrm{gas}}Z$ weighted by the local stellar luminosity.

This relation between surface density, metallicity, and IRX is very closely related to the relations between IRX and luminosity, and between IRX and stellar mass—these, in turn, are key to interpreting the color-magnitude diagram of galaxies in terms of models for the build-up of stellar mass (Labbe et al. 2007; Noeske et al. 2007). If the sizes of late-type galaxies are nearly constant or correlated with the total SFR, then the gas surface densities are also correlated with total SFR. In this case, the relation between IRX and gas surface density, a more direct probe of the physical conditions related to attenuation, is almost trivially related to the well-known correlation between IRX and SFR (Martin et al. 2005). A similar argument may be made for the stellar mass surface density and total stellar mass. Interestingly, the scatter in the relation presented here does not appear to be significantly less than the scatter in the IRX-L_{SF} relation (see Johnson et al. 2007b).

If, however, the measured attenuation does prove a useful probe of the global $\Sigma_{\mathrm{gas}}Z$, then the measured distribution of attenuation may provide a strong constraint on models of galaxy evolution, since both gas surface density and metallicity are intimately related to star birth and star death (Martin et al. 2007).

7. CONCLUSIONS

1. For $D_n(4000) < 1.7$ we find little evidence that scatter in the IRX-β diagram is caused primarily by variations in UV color with the SFH of the stellar population, as suggested by Kong et al. (2004). However, IRX may be affected by the SFH, which could mask such an effect.

2. We assess the utility of the IRX-β relation for determining dust attenuation at high redshift using UV colors alone. While the scatter is small, the large slope makes the derived IRX very sensitive to even small errors in the UV color ($\sim$0.1 mag). These may be random (due to measurement errors) or systematic, for example, due to the method used to K-correct the data. Furthermore, significant uncertainty in the determination of the bolometric IR luminosity makes even the low-redshift relation uncertain.

3. We use the UV through IR data to show how the entire spectral energy distribution (not just a single color) varies as a function of the relevant galaxy parameters IRX, $D_n(4000)$, and M_*. This results in high-quality, low-resolution 1375 Å through 70 μm average SEDs normalized by M_* for different ranges of IRX, $D_n(4000)$, and M_*. Such average SEDs show a variation of the 3.6 μm mass-to-light ratio with $D_n(4000)$, when stellar masses are estimated from optical data following Kauffmann et al. (2003a). They also show the strong variation in the UV and IR specific luminosities with these quantities, although the variation with M_* is driven largely by the correlation of SFH and attenuation with M_* (which might be expected to change with redshift).

4. We have used these average SEDs to derive a low-resolution dust attenuation curve for blue-sequence galaxies, for several different ranges of $D_n(4000)$. The accuracy of the attenuation curves is limited by the variation of the relation between IRX and the true attenuation $A_{\rm fuv}$, but the derived attenuation curves are consistent with a $\lambda^{-0.7}$ law. To investigate possible changes in the attenuation law as a function of metallicity or PAH abundance, we repeat the analysis, splitting galaxies by their stellar mass. We find no significant differences as a function of mass, although the uncertainties are large.

5. IRX is correlated with both stellar mass surface density and gas-phase metallicity (as determined by Kauffmann et al. [2003b] and Tremonti et al. [2004], respectively), although the latter correlation appears weak for a given narrow range of stellar mass surface density. To the extent that the stellar mass surface density is related to the gas surface density, IRX then probes the causes of dust attenuation, and this relation allows the accurate calculation of attenuation in models of galaxy formation. This, in turn, will allow for the consistent comparison of photometric data to these models. Conversely, the attenuation can be used to probe the variation in the surface density and metallicity as a function of time through observations of high-redshift galaxies in the rest-frame UV and mid- to far-IR.

B. D. J. would like to thank A. Basu-Zych, S. Salim, A. Boselli, S. Boissier, and L. Cortese for comments that improved the paper. B. D. J. was supported by NASA GSRP grant NNG-05GO43H. *GALEX* (*Galaxy Evolution Explorer*) is a NASA Small Explorer, launched in 2003 April. We gratefully acknowledge NASA's support for construction, operation, and science analysis for the *GALEX* mission, developed in cooperation with the Centre National d'Etudes Spatiales of France and the Korean Ministry of Science and Technology. This work is based in part on observations made with the *Spitzer Space Telescope*, which is operated by the Jet Propulsion Laboratory, California Institute of Technology, under a contract with NASA. In particular, the publicly available *Spitzer* data obtained by the SWIRE team have been essential to this work. Funding for the SDSS and SDSS-II has been provided by the Alfred P. Sloan Foundation, the Participating Institutions, the National Science Foundation, the Department of Energy, the National Aeronautics and Space Administration, the Japanese Monbukagakusho, the Max Planck Society, and the Higher Education Funding Council for England. The SDSS Web site is http://www.sdss.org. The SDSS is managed by the Astrophysical Research Consortium for the Participating Institutions. The Participating Institutions are the American Museum of Natural History, Astrophysical Institute Potsdam, University of Basel, University of Cambridge, Case Western Reserve University, University of Chicago, Drexel University, Fermilab, the Institute for Advanced Study, the Japan Participation Group, Johns Hopkins University, the Joint Institute for Nuclear Astrophysics, the Kavli Institute for Particle Astrophysics and Cosmology, the Korean Scientist Group, the Chinese Academy of Sciences (LAMOST), Los Alamos National Laboratory, the Max Planck Institute for Astronomy (MPIA), the Max Planck Institute for Astrophysics (MPA), New Mexico State University, Ohio State University, University of Pittsburgh, University of Portsmouth, Princeton University, the United States Naval Observatory, and the University of Washington.

REFERENCES

Balogh, M. L., Morris, S. L., Yee, H. K. C., Carlberg, R. G., & Ellingson, E. 1999, ApJ, 527, 54
Bell, E. F. 2002, ApJ, 577, 150
———. 2003, ApJ, 586, 794
Bell, E. F., Gordon, K. D., Kennicutt, R. C., & Zaritsky, D. 2002, ApJ, 565, 994
Bell, E. F., et al. 2004, ApJ, 608, 752
Blanton, M. R., & Roweis, S. 2007, AJ, 133, 734
Boissier, S., Boselli, A., Buat, V., Donas, J., & Milliard, B. 2004, A&A, 424, 465
Boissier, S., et al. 2007, ApJS, 173, 524
Brinchmann, J., Charlot, S., White, S. D. M., Tremonti, C., Kauffmann, G., Heckman, T., & Brinkmann, J. 2004, MNRAS, 351, 1151
Bruzual, G., & Charlot, S. 2003, MNRAS, 344, 1000
Buat, V., & Xu, C. 1996, A&A, 306, 61
Buat, V., et al. 2005, ApJ, 619, L51
Burgarella, D., et al. 2005, ApJ, 619, L63
Calzetti, D., et al. 2007, ApJ, 666, 870
———. 2005, ApJ, 633, 871
Charlot, S., & Fall, S. M. 2000, ApJ, 539, 718
Cortese, L., et al. 2006, ApJ, 637, 242
Croton, D. J., et al. 2006, MNRAS, 365, 11
Dale, D. A., & Helou, G. 2002, ApJ, 576, 159
Dale, D. A., Helou, G., Contursi, A., Silbermann, N. A., & Kolhatkar, S. 2001, ApJ, 549, 215
Dale, D. A., et al. 2005, ApJ, 633, 857
De Lucia, G., Springel, V., White, S. D. M., Croton, D., & Kauffmann, G. 2006, MNRAS, 366, 499
Donas, J., et al. 2007, ApJS, 173, 597
Draine, B. T., & Li, A. 2007, ApJ, 657, 810
Faber, S. M., et al. 2007, ApJ, 665, 265
Gil de Paz, A., et al. 2007, ApJS, 173, 185
Gordon, K. D., Clayton, G. C., Witt, A. N., & Misselt, K. A. 2000, ApJ, 533, 236
Heckman, T. M., Robert, C., Leitherer, C., Garnett, D. R., & van der Rydt, F. 1998, ApJ, 503, 646
Helou, G., Khan, I. R., Malek, L., & Boehmer, L. 1988, ApJS, 68, 151
Isobe, T., Feigelson, E. D., Akritas, M. G., & Babu, G. J. 1990, ApJ, 364, 104
Johnson, B. D., et al. 2006, ApJ, 644, L109
———. 2007a, ApJS, 173, 377
———. 2007b, ApJS, submitted

Kauffmann, G., et al. 2007, ApJS, 173, 357
———. 2003a, MNRAS, 341, 33
———. 2003b, MNRAS, 341, 54
Kennicutt, R. C. 1998a, ARA&A, 36, 189
Kennicutt, Jr., R. C. 1998b, ApJ, 498, 541
Kong, X., Charlot, S., Brinchmann, J., & Fall, S. M. 2004, MNRAS, 349, 769
Labbe, I., et al. 2007, ApJ, 665, 944
MacArthur, L. A. 2005, ApJ, 623, 795
Madau, P., Ferguson, H. C., Dickinson, M. E., Giavalisco, M., Steidel, C. C., & Fruchter, A. 1996, MNRAS, 283, 1388
Martin, D. C., et al. 2005, ApJ, 619, L59
———. 2007, ApJS, 173, 415
Meurer, G. R., Heckman, T. M., & Calzetti, D. 1999, ApJ, 521, 64
Morrissey, P., & Seibert, M. 2007, ApJS, 173, 682
Noeske, K. G., et al. 2007, ApJ, 660, L43
Panuzzo, P., Granato, G. L., Buat, V., Inoue, A. K., Silva, L., Iglesias-Páramo, J., & Bressan, A. 2007, MNRAS, 375, 640
Pierini, D., Gordon, K. D., Witt, A. N., & Madsen, G. J. 2004, ApJ, 617, 1022
Reddy, N. A., Steidel, C. C., Fadda, D., Yan, L., Pettini, M., Shapley, A. E., Erb, D. K., & Adelberger, K. L. 2006, ApJ, 644, 792
Salim, S. 2007, ApJS, 173, 267
Schiminovich, D., et al. 2005, ApJ, 619, L47
Seibert, M., et al. 2005, ApJ, 619, L55
Somerville, R. S., Primack, J. R., & Faber, S. M. 2001, MNRAS, 320, 504
Tremonti, C. A., et al. 2004, ApJ, 613, 898
Wang, B., & Heckman, T. M. 1996, ApJ, 457, 645
Witt, A. N., & Gordon, K. D. 2000, ApJ, 528, 799
Xu, C., Buat, V., Boselli, A., & Gavazzi, G. 1997, A&A, 324, 32
Zheng, X. Z., Dole, H., Bell, E. F., Le Floc'h, E., Rieke, G. H., Rix, H.-W., & Schiminovich, D. 2007, ApJ, 670, 301